# Internal Boundary Control in Lane-free Automated Vehicle Traffic: Comparison of Approaches via Microscopic Simulation

Milad Malekzadeh[1*], Dimitrios Troullinos[1], Ioannis Papamichail[1], Markos Papageorgiou[1,2], Klaus Bogenberger[3]

[1]Dynamic Systems and Simulation Laboratory, Technical University of Crete, Chania 73100, Greece

[2]Faculty of Maritime and Transportation, Ningbo University, Ningbo, China

[3]Technical University of Munich, Chair of Traffic Engineering and Control, Munich, Germany

*Corresponding author (email: mmalek@dssl.tuc.gr)

**Abstract-** The recently introduced *TrafficFluid* concept proposes that automated vehicles drive lane-free, thus enabling capacity sharing between the two opposite road directions via real-time Internal Boundary Control (IBC). This novel traffic control measure was demonstrated, using macroscopic traffic flow models, to deliver unprecedented improvements of traffic flow efficiency. The present study completes and validates the IBC concept in a much more realistic way via microscopic simulation and active internal boundary moving, using the SUMO-based *TrafficFluid-Sim* simulation tool. To effectuate IBC, a Linear Quadratic Regulator (LQR), which is a feedback control scheme, is employed. In addition, to enhance the performance of the LQR controller, a feedforward term, accounting for external disturbances, i.e. entering flow and on-ramp flows, is also designed, leading to an augmented LQR-FF control scheme. The LQR and LQR-FF controllers are tested and compared in the created realistic environment, demonstrating how IBC may operate in practice to combat traffic congestion on highways.

**Keyword-** Internal Boundary control; LQR; Feedforward; TrafficFluid-Sim; Microscopic simulation.

## 1. Introduction

Despite the development and partial deployment of traffic management systems (Papageorgiou et al., 2003; Kurzhanskiy and Varaiya, 2010), traffic congestion on freeway and urban road networks continues to be a major problem for society. Existing and emerging vehicle automation and communication systems enable innovative traffic management actions that may further mitigate traffic congestion (Diakaki et al., 2015; Papamichail et al., 2019). Further

advances facilitate a number of prototype vehicles to keep track of their surroundings and make reliable and efficient autonomous driving decisions. Furthermore, vehicle communication enables vehicles to communicate with each other and with the infrastructure, which opens the door for a variety of enhanced or additional applications (Rostami-Shahrbabaki et al., 2023).

Recently, Papageorgiou et al. (2021) put forward the *TrafficFluid* concept, a forward-thinking paradigm for vehicular traffic that is suitable for traffic with a high percentage of vehicles outfitted with high-level automation and communication systems. A distinguishing feature of TrafficFluid is lane-free traffic of connected and automated vehicles (CAV), which allows for an improved exploitation of the road infrastructure. In this context, it becomes possible to introduce Internal Boundary Control (IBC), a novel and highly promising control measure, which relies on the fact that, in lane-free traffic, the traffic flow and capacity exhibit incremental changes in accordance with corresponding incremental changes of the road width, as demonstrated in (Papamichail et al., 2023). Thus, by virtually shifting the internal boundary that separates the two directions of traffic on highways or arterials, the total crossroad capacity can be flexibly shared between them in real-time, depending on the prevailing traffic conditions. The boundary-shifting information is sent to CAV so that they can drive in accordance with the changed internal road boundary. Real-time IBC could potentially be widely used for lane-free CAV traffic on the numerous arterial or highway infrastructures that feature different demand levels in each direction, in time or in space, so as to drastically reduce or even eliminate congestion.

Malekzadeh et al. (2021a) studied the features of IBC, illustrating the underlying mechanism and improvement potential through formulating and resolving an open-loop optimal control problem in form of a convex Quadratic Programming (QP) problem, aiming to minimize the total time spent by all vehicles in both directions of the highway. This strategy can be cast in a Model Predictive Control (MPC) frame, along with a demand prediction module for real-time operation. Though, it is preferable to use simpler real-time methods which achieve similar levels of efficacy, but do not require online traffic flow modelling and demand prediction. To this end, Malekzadeh et al. (2021b) developed a feedback-based Linear-Quadratic Regulator (LQR) for IBC, which strives to keep the relative density of the two traffic directions near their nominal value (close to capacity). This closed-loop LQR approach was demonstrated, using macroscopic simulation, to be almost as efficient as the open-loop optimal control solution,

without requiring an accurate model or demand forecasts (Malekzadeh et al., 2021b; Malekzadeh et al., 2023).

As already practiced in other applications (Marinaki and Papageorgiou, 2005; Papageorgiou, et al., 2015), LQR performance can be enhanced in the presence of external disturbances by adding a feedforward term to the basic feedback controller. In the IBC context, such an addition is considered in this paper to mitigate the effect of entering and on-ramp flows on the controller performance. The stationary LQR feedback and feedforward gains are designed offline; then, in real-time operation, the control input is computed as the sum of: (i) the state measurements multiplied with the feedback gain and (ii) the inflow measurements multiplied with the feedforward gain. Following this procedure, LQR-Feedforward (LQR-FF) is employed, tested and compared for IBC in this study.

Up to this point, the mentioned IBC control schemes were applied and tested using macroscopic traffic flow models. Microscopic implementation is a crucial step to investigate, beyond the basic macroscopic concept, the suitability, feasibility, robustness and efficiency of the IBC measure and the related control strategies in realistically emulated vehicle behavior and emerging traffic conditions. The investigation addresses open questions, such as: Can lane-free driving CAV timely and safely evacuate internal road zones assigned to the other traffic direction in real-time? Can CAV efficiently exploit additional road zones assigned to their direction? Can CAV drive safely on a highway where the internal boundary is changing over space? How do flow and capacity of a traffic direction relate to narrowing or widening of the road infrastructure? What is an appropriate space resolution for IBC application, and how should different sharing decisions be implemented in space? What is an appropriate time-step for real-time IBC application? Is the achievable efficiency increase as high as indicated by the afore-mentioned macroscopic investigations? Is the macroscopically derived controller robust to the inevitable subtleties and system "noise" introduced by a realistic microscopic environment?

In this regard, a lane-free extension of the well-known microscopic simulator SUMO (Lopes et al., 2018), called *TrafficFluid-Sim* (Troullinos et al., 2021), has been developed for use in various TrafficFluid-related investigations. Additional functionalities had to be specifically developed to facilitate the use of changing internal boundaries, some of which are outlined as part of future work by Troullinos et al. (2022). Also, in the microscopic environment, the

vehicles must follow a lane-free movement strategy. In this context, the ad-hoc model suggested by Malekzadeh et al. (2022) for a ring-road is modified here to incorporate policies for on- and off-ramps in highway scenarios.

In summary, the present work significantly extends the state-of-the-art and state-of-knowledge regarding the innovative IBC measure. It is the first to consider IBC at a microscopic level, aiming to:

i) advance the IBC method by developing the microscopic application procedures that are necessary for actual IBC application in practice; and

ii) verify the macroscopic assumptions and confirm the excellent IBC performance in a very realistic environment.

These are important contributions, without which the IBC concept would not be complete. To enable the above items, several substantial developments were necessary, including: IBC implementation procedures enabling smooth vehicle advancing vis-à-vis a variable-width road; design of appropriate vehicle movement strategy; IBC-induced extensions of the lane-free microscopic simulator TrafficFluid-Sim, to name just a few. Furthermore, this study progresses also the kernel IBC methodology by developing an extension of our previous controller with a feedforward term, the reasoning, implications and advantages of which are thoroughly examined using various criteria.

The remainder of the paper is organized as follows: Section 2 covers some background for understanding the IBC concept and LQR; and presents the novel feedforward term design. Information on TrafficFluid-Sim and its extension to accommodate IBC implementation are given in Section 3. Section 4 outlines the extended ad-hoc vehicle moving strategy. Section 5 presents the simulation results, while Section 6 concludes the paper.

## 2. Internal Boundary Control Background and Controller Design

This section provides an overview of the IBC macroscopic modelling, the LQR and the novel LQR-FF control design, which are essential for proper understanding of the IBC application. For more details, see (Malekzadeh et al., 2021a; Malekzadeh et al., 2021b).

## 2.1 Macroscopic Modelling for IBC

Macroscopic IBC modelling was based on the expectation, to be verified in this paper, that lane-free traffic does not entail any significant modifications to the fundamental components of existing macroscopic traffic flow models. An extended version of CTM (Cell Transmission Model), a first-order dynamic traffic flow model with a triangular fundamental diagram (Daganzo, 1994), was considered for control design (Malekzadeh et al., 2021b).

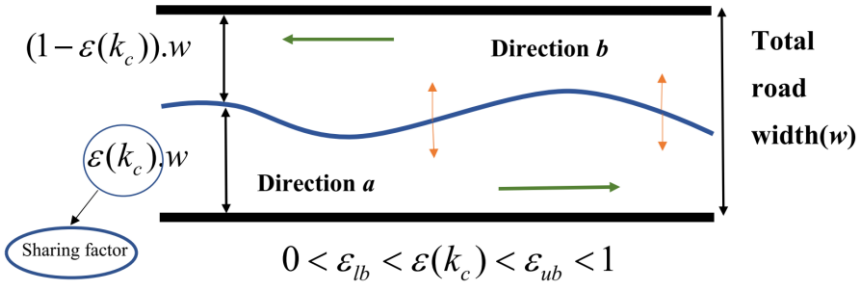


Fig. 1: Space-time flexible internal road boundary.

Figure 1 shows a road stretch with two directions of traffic: direction $a$ from left to right; and direction $b$ from right to left. IBC implies that the internal boundary separating the two directions may be changed flexibly in space and time according to the traffic conditions. For macroscopic modelling, rather than using a space-continuous separation curve as in Figure 1, the road stretch is partitioned into $n$ sections, with respective lengths $L_i$ (of some 500 m), and the total road width (both directions) $w$, which is assumed constant over all sections for simplicity, can be shared in real-time, independently for each section, between the two traffic directions. As a result, each direction is assigned a corresponding road width $w_i^a = \varepsilon_i \cdot w$ and $w_i^b = (1-\varepsilon_i) \cdot w$, where $0 \le \varepsilon_i \le 1$ is the *sharing factor* per section $i = 1, 2, \ldots, n$, to be specified in real-time as a control input by the internal boundary controller. The total (both directions) section capacity $q_{cap}$, as well as the total critical density $\rho_{cr}$ and the total jam density $\rho_{\max}$, are accordingly shared at each section between the two traffic directions $a$ and $b$. Based on the derivation presented by Malekzadeh, et al. (2021a), these quantities are given by direction from the following relations

$$
\begin{aligned}
&q_{i,cap}^a(\varepsilon_i) = \varepsilon_i \cdot q_{cap},\ q_{i,cap}^b(\varepsilon_i) = (1-\varepsilon_i) \cdot q_{cap} \\
&\rho_{i,cr}^a(\varepsilon_i) = \varepsilon_i \cdot \rho_{cr},\ \rho_{i,cr}^b(\varepsilon_i) = (1-\varepsilon_i) \cdot \rho_{cr} \\
&\rho_{i,\max}^a(\varepsilon_i) = \varepsilon_i \cdot \rho_{\max},\ \rho_{i,\max}^b(\varepsilon_i) = (1-\varepsilon_i) \cdot \rho_{\max}
\end{aligned}
\tag{1}
$$

While applying IBC, it is not permissible to fully close any of the two directions; hence, the designated road width in any direction must never be narrower than the greatest width of vehicles travelling on the road, leading to stricter constraints on the sharing factors, as follows

$$0 < \varepsilon_{lb} \le \varepsilon_i \le \varepsilon_{ub} < 1 \tag{2}$$

where $\varepsilon_{lb} \cdot w$ and $(1-\varepsilon_{ub}) \cdot w$ are the minimum admissible widths to be assigned to directions $a$ and $b$, respectively.

Another restriction to be applied to the sharing factors concerns the time-delay needed to evacuate traffic on the direction that receives a restricted width, compared to the previous control time-step. Obviously, the time-delay in applying the new sharing factor should only take place for the direction of traffic that is being widened in comparison to the previous control interval. In contrast, the restricted direction should promptly be provided with the narrower width, so that CAV therein can evacuate the limited-width region removed. Assume that the required time-delay is smaller than or equal to the control time interval $T_c$; then, the time-delay requirement is automatically fulfilled for each section $i$, if the sharing factors that are actually applied to the two directions, i.e. $\varepsilon_i^a$ and $\varepsilon_i^b$, respectively, are calculated as follows

$$\begin{aligned} \varepsilon_i^a(k_c) &= \min\left\{\varepsilon_i(k_c), \varepsilon_i(k_c-1)\right\} \\ \varepsilon_i^b(k_c) &= \min\left\{1-\varepsilon_i(k_c), 1-\varepsilon_i(k_c-1)\right\} \end{aligned} \tag{3}$$

where $k_c = 0,1,\ldots$ is the discrete control time index. It should be mentioned that the notation $\varepsilon_i^a(k_c)$ and $\varepsilon_i^b(k_c)$ indicates that the sharing factors are applied for the duration of the control time interval $[k_c \cdot T_c, (k_c+1) \cdot T_c)$. The above equations may be readily extended if the required time-delay is a multiple of the control time interval $T_c$.

In conventional traffic management, the traffic density (in veh/km) gives a clear indication of the state of traffic, depending on its value compared to the critical density: free-flow traffic (when density is lower than critical density), critical traffic (when density is around critical density) or congested traffic (when density is higher than critical density). However, as opposed to having a constant critical density for each direction and section, IBC has the critical density determined by the sharing factor (see (1)); hence altering dynamically according to the control action. Consequently, the sole use of the density value does not provide a consistent view of the traffic conditions in a given section in the presence of IBC.

To tackle this problem, the following relations define the relative densities (dimensionless) per section and per direction. The relative density of section $i$ and direction $a$ or $b$ is obtained by dividing the corresponding traffic density with the corresponding critical density, which, on its turn, depends on the sharing factor (see (1)) prevailing during the last time-step, as follows

$$\tilde{\rho}_i^a(k) = \frac{\rho_i^a(k)}{\varepsilon_i(k-1)\rho_{cr}},\ \tilde{\rho}_i^b(k) = \frac{\rho_i^b(k)}{(1-\varepsilon_i(k-1))\rho_{cr}}. \tag{4}$$

The relative densities enable consistent assessment of the traffic conditions in the IBC context. Specifically, if the relative density of a section and direction is less than 1, it reflects under-critical (free-flow) traffic conditions; if it is around 1, it reflects capacity flow; and if it is greater than 1, it reflects over-critical (congested) traffic conditions.

### 2.2 LQR Design for IBC

CTM contains one state equation per section and direction, which is the conservation equation describing the evolution of traffic density. Although the conservation equation is linear, the flow variables included on its right-hand side are nonlinear functions of density. Therefore, Malekzadeh et al. (2021b) proffered linearization of the CTM dynamic equations around a nominal point. In addition, as densities are replaced by relative densities according to (4) as state variables, the one-step retarded control input was attached as a new state variable via $\gamma_i(k+1) = \varepsilon_i(k),\ \ i = 1,2,\ldots,n.$ This way, the following linearized state-space model was derived in (Malekzadeh, et al., 2021b)

$$\Delta\mathbf{x}(k+1) = \hat{\mathbf{A}}\Delta\mathbf{x}(k) + \hat{\mathbf{B}}\Delta\mathbf{u}(k) \tag{5}$$

where $\Delta\mathbf{x}(k) = [\Delta\tilde{\rho}_1^a(k), \Delta\tilde{\rho}_1^b(k), \Delta\gamma_1(k), ..., \Delta\tilde{\rho}_n^a(k), \Delta\tilde{\rho}_n^b(k), \Delta\gamma_n(k)]^T$ is the state vector and $\Delta\mathbf{u}(k) = \Delta\boldsymbol{\varepsilon}(k)$ is the control vector, whereby $\Delta\boldsymbol{\varepsilon}(k) = [\Delta\varepsilon_1(k), \ldots, \Delta\varepsilon_n(k)]^T$. Also, $\Delta(.)(k) = (.)(k) - (.)^N$, the superscript $N$ denoting the nominal values, while it was assumed for simplicity that $\Delta(.)(k) = 0$ for all external disturbances (upstream mainstream inflows, as well as the on-ramp flows, of each direction). $\hat{\mathbf{A}} \in \mathbb{R}^{3n\times 3n}$ and $\hat{\mathbf{B}} \in \mathbb{R}^{3n\times n}$ are the time-invariant state and input matrices, respectively, which result from the linearization, while $\Delta\mathbf{x} \in \mathbb{R}^{3n}$ and $\Delta\mathbf{u} \in \mathbb{R}^n$.

As is well-known (see, e.g. (Treiber and Kesting, 2013)), the time-step of system (5) must be determined according to the section lengths and the free flow speed for numerical stability (e.g., $T = 10\,s$ for $L = 0.5\,km$), according to the Courant-Friedrichs-Lewy (CFL) condition; Courant

et al., 1928. If the control time-step is taken as a multiple of the model time-step, i.e. $T_c = MT$, where $M$ is an integer, then the discrete control time index is $k_c = \lfloor kT/T_c \rfloor$. Thus, the linear state-space equation (5) may be changed as follows, in order to be based on the control time-step $T_c$,

$$\Delta\mathbf{x}(k_c+1) = \mathbf{A}\Delta\mathbf{x}(k_c) + \mathbf{B}\Delta\mathbf{u}(k_c) \tag{6}$$

where $\mathbf{A} = \hat{\mathbf{A}}^M$, and $\mathbf{B} = (\hat{\mathbf{A}}^{M-1} + \hat{\mathbf{A}}^{M-2} + .... + \mathbf{I})\hat{\mathbf{B}}$.

To enable the derivation of a time-invariant LQR for the LTI (Linear Time-Invariant) system (6), Malekzadeh et al. (2021b) proposed minimization of the infinite time-horizon quadratic criterion

$$J = \frac{1}{2}\sum_{k_c=0}^{\infty}\left[\Delta\mathbf{x}^T(k_c)\mathbf{Q}\Delta\mathbf{x}(k_c) + \Delta\mathbf{u}^T(k_c)\mathbf{R}\Delta\mathbf{u}(k_c)\right] \tag{7}$$

where $\mathbf{Q} \in \mathbb{R}^{3n\times 3n}$ is a diagonal positive semidefinite matrix, and $\mathbf{R} \in \mathbb{R}^{n\times n}$ is a diagonal positive definite matrix. The first term penalizes deviations of the state variables from zero, i.e. deviations of $\tilde{\rho}_i^a(k_c)$, $\tilde{\rho}_i^b(k_c)$, $\gamma_i(k_c)$, $i = 1, 2, \ldots, n$, from their respective nominal values. The second term penalizes deviations of the control inputs from the nominal values.

The controller is set to operate the system near capacity by setting the nominal value of relative densities on both directions to 1, which is beneficial for traffic efficiency. Due to the quadratic penalty terms, the controller attempts to reduce the strong deviation of density from the critical density at certain sections, which works to alleviate traffic congestion. On the other hand, by setting the nominal value for the sharing factors to 0.5, the internal boundaries are allowed to shift moderately if density deviations are moderate. Thus, minimization of the second term in (7) mitigates deviations of the sharing factors from 0.5 and balances these deviations in space and time, which is a secondary operational sub-objective, as unnecessarily strong internal boundary changes over space and time should be suppressed.

The optimal controller minimizing the criterion (7) subject to the model (6) is given by a linear state-feedback control law of the form $\Delta\mathbf{u}(k_c) = \mathbf{K}\Delta\mathbf{x}(k_c)$, where $\mathbf{K} \in \mathbb{R}^{n\times 3n}$ is a constant gain matrix given by

$$\mathbf{K} = (\mathbf{R} + \mathbf{B}^T\mathbf{P}\mathbf{B})^{-1}\mathbf{B}^T\mathbf{P}\mathbf{A} \tag{8}$$

and $\mathbf{P}$ is the unique positive semidefinite solution of the discrete-time algebraic Riccati equation. To drop the nominal point from the controller, the differential form of the controller is given as follows

$$\mathbf{u}(k_c) = \mathbf{u}(k_c - 1) + \mathbf{K}(\mathbf{x}(k_c) - \mathbf{x}(k_c - 1)) . \tag{9}$$

The control input is truncated if it exceeds the bounds (2). This LQR was applied in (Malekzadeh, et al., 2021b) to the nonlinear extended CTM as ground truth, with control inputs $\varepsilon_i^a(k_c)$ and $\varepsilon_i^b(k_c)$ according to (3) being directly applied to the nonlinear macroscopic model. This first successful test opened the way for a more detailed and realistic implementation and evaluation, using lane-free microscopic simulation, where the sharing factors must first be transformed to a continuous internal boundary curve (as in Figure 1); while lane-free driving vehicles are called to respect the internal boundary that changes at every time-step $T_c$, according to the control decisions. These developments are presented in the following sections.

### 2.3 LQR-Feedforward (LQR-FF) Design for IBC

The LQR above was derived under the assumption that $\Delta(.)(k) = 0$ for all external disturbances (mainstream inflows and on-ramp flows of each direction); i.e., that the disturbances remain constant at their nominal values. Clearly, the external inflows are not constant in highway traffic, but feature strong variations during the day (peak and off-peak periods). LQR may nevertheless be efficient thanks to its feedback structure that reacts to the changes of traffic density caused by the inflows, without explicitly accounting for the actual inflow values. Having said that, it is worth investigating whether an extended LQR, namely LQR-FF, that includes, beyond the state feedback, also a feedforward term to explicitly account for the current inflow values, might provide additional benefits. Further details on the design and applications of LQR-FF may be found in (Marinaki and Papageorgiou, 2005; Papageorgiou, et al., 2015).

To derive such an extended LQR-FF, we assume that, also for the disturbances, $\Delta(.)(k)$ are non-zero, hence we have the following augmented linearized system equation instead of (5)

$$\Delta\mathbf{x}(k+1) = \hat{\mathbf{A}}\Delta\mathbf{x}(k) + \hat{\mathbf{B}}\Delta\mathbf{u}(k) + \hat{\mathbf{D}}\Delta\mathbf{d}(k) \tag{10}$$

where $\Delta\mathbf{d}(k) = [\Delta q_0^a(k), \Delta r_1^b(k), \Delta r_2^a(k), \Delta r_2^b(k), ..., \Delta r_n^a(k), \Delta q_{n+1}^b(k)]^T$. $q_0^a$ and $q_{n+1}^b$ are the upstream entering flows for the directions $a$ and $b$, respectively, while $r_i^a$ and $r_i^b$ denote the

on-ramp flows for section $i$ (if any) for the directions $a$ and $b$, respectively. Thus, the state-space equation (6) is also changed as follows, in order to be based on the control time-step $T_c$,

$$\Delta\mathbf{x}(k_c+1) = \mathbf{A}\Delta\mathbf{x}(k_c) + \mathbf{B}\Delta\mathbf{u}(k_c) + \mathbf{D}\Delta\mathbf{d}(k_c) \tag{11}$$

where $\mathbf{D} = (\hat{\mathbf{A}}^{M-1} + \hat{\mathbf{A}}^{M-2} + .... + \mathbf{I})\hat{\mathbf{D}}$.

To derive a time-invariant controller, we will start by assuming that the disturbance is constant, i.e., that $\Delta\mathbf{d}(k_c) = \Delta\bar{\mathbf{d}}$. This is because consideration of a time-varying disturbance has two annoying implications: (i) the need to predict the future values of the disturbance; and, most importantly, (ii) due to finite horizon of the prediction, the resulting LQR and the feedforward term become time-varying and must be computed repeatedly online (Marinaki and Papageorgiou, 2005). Therefore, if the disturbance does not vary fast over time, we can simplify the controller design and application by considering it, in the design phase, as a constant. Then, considering minimization of the same objective criterion (7) with the extended system (11) yields (Marinaki and Papageorgiou, 2005) the optimal controller

$$\Delta\mathbf{u}(k_c) = \mathbf{K}\Delta\mathbf{x}(k_c) - \mathbf{F}\Delta\bar{\mathbf{d}} \tag{12}$$

where $\mathbf{F} = \mathbf{\Psi}(\mathbf{I} - \mathbf{Z})^{-1}\mathbf{PD}$, and $\mathbf{\Psi} = [\mathbf{R} + \mathbf{B}^{\mathbf{T}}\mathbf{PB}]^{-1}\mathbf{B}^{\mathbf{T}}$, $\mathbf{Z} = \mathbf{A}^{\mathbf{T}}\left[\mathbf{I} - \mathbf{PB\Psi}\right]$, where $\mathbf{F}$ is a constant feedforward gain matrix.

Assuming now that the disturbance is not constant but slowly changing, to account for the time-variations of the inflows, we may render the feedforward term in (12) time-varying by replacing $\Delta\bar{\mathbf{d}}$ in (12) by $\Delta\mathbf{d}(k_c)$, which yields the LQR-FF as follows

$$\Delta\mathbf{u}(k_c) = \mathbf{K}\Delta\mathbf{x}(k_c) - \mathbf{F}\Delta\mathbf{d}(k_c). \tag{13}$$

Eventually, LQR-FF may be taken in differential form

$$\mathbf{u}(k_c) = \mathbf{u}(k_c - 1) + \mathbf{K}(\mathbf{x}(k_c) - \mathbf{x}(k_c - 1)) - \mathbf{F}(\Delta\mathbf{d}(k_c) - \Delta\mathbf{d}(k_c - 1)). \tag{14}$$

Clearly, LQR-FF requires, beyond state measurements, also external inflow measurements for real-time operation. By employing microscopic simulation, this study evaluates the proposed controller extension and its features. One particular issue to be evaluated, along with possible remedies, is the impact of noise, that is typically present in flow measurements, on the control signal, see Section 5.1.

## 3. Lane-Free Microscopic Implementation and Simulation of IBC

In the recent past, after introducing the innovative IBC concept, a couple of papers addressed IBC regulator design and testing, accounting for several requirements. These works were based on reasonable, but not yet verified assumptions regarding the macroscopic implications and application conditions of IBC. Through a meticulous design and examination of the microscopic aspects of IBC, this study extends and completes the IBC methodology and investigates its feasibility and practicality.

As mentioned, the IBC concept was tested in previous works macroscopically, whereby the sharing factors $\varepsilon_i$ were implemented directly in (1) as control inputs. However, the real physical control input in practice is the space-dependent internal boundary curve (blue line in Fig. 1), which needs to be specified appropriately, based on the controller decisions, i.e., the sharing factors $\varepsilon_i$ by section. It should be noted that the internal boundary curve should be smooth, to allow for lane-free driving vehicles to smoothly and safely adapt to internal boundary changes encountered on their way. The same requirements apply to the microscopic simulator used for IBC testing; hence, microscopic IBC evaluation is deemed to be close to real implementation. Experimental evaluation is performed with TrafficFluid-Sim (Troullinos et al., 2021), a lane-free extension of the well-known microscopic simulator SUMO (Lopes et al., 2018). For IBC, additional functionalities had to be developed in order to facilitate the possibility of changing internal boundaries. Some of these extensions are outlined as part of future work by Troullinos et al. (2022).

### 3.1 Lateral Boundaries in Lane-Free Environments

Consider a network with multiple routes, e.g., a highway with on-ramps and off-ramps. Each vehicle entering the network (at the upstream boundary or at an on-ramp) is assigned a specific itinerary according to its destination (downstream boundary or an off-ramp). In conventional lane-based traffic, the vehicle would need to undertake appropriate lane-changing operations in order to follow its itinerary. In a lane-free environment, realization of the prescribed itinerary calls for appropriate considerations within the vehicle movement strategy, to be detailed in Section 4. In addition, a corresponding admissible movement corridor, delineated by smooth left and right boundaries, is designed that limits the vehicle's lateral placement appropriately. For example, a vehicle entering from an on-ramp needs to first merge appropriately in the main

highway. To this end, its movement boundaries are designed with the use of sigmoid functions that specify the laterally admissible positions for the associated itinerary as a function of longitudinal space $x$ (Fig. 2).

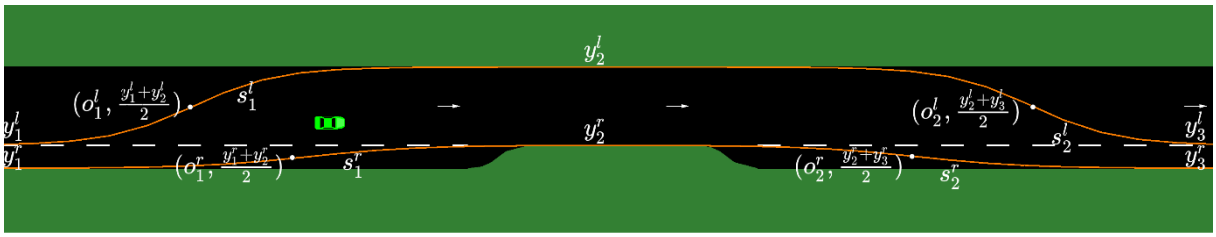


Fig. 2: Illustration of the boundaries for vehicles entering from an on-ramp and scheduled to exit from an off-ramp

For every itinerary, the boundaries (left and right) are designed generically with a set of parameters that dictate their shape using hyperbolic tangent functions. In Fig. 2, we showcase the boundaries in TrafficFluid-Sim and illustrate the design procedure through relevant parameters for an itinerary where vehicles enter from an on-ramp; drive on the main road for a while; and then exit through an off-ramp located downstream. The $l$, $r$ superscripts on the parameters indicate elements relevant to the left or right boundary, respectively, and both boundaries are designed following the same principle.

To clarify the design process, we focus on the left boundary from the perspective of the vehicle, which is partitioned into 3 distinct phases corresponding to changes in the lateral availability of the road. First, we define the 3 distinct lateral levels $y_1^l, y_2^l, y_3^l$ as shown in the figure, according to the itinerary that the vehicles shall follow; i.e., $y_1^l$ is set according to the left boundary of the on-ramp's acceleration lane; $y_2^l$ is set according to the left boundary of the main road; and $y_3^l$ is set according to the left boundary of the off-ramp's deceleration lane. These three levels need to be connected via a smooth line to form the complete left boundary of the itinerary to be considered by the corresponding vehicles, as they move longitudinally through the road network. To connect the three levels, longitudinal offset locations are specified, imposing where (longitudinally) the smooth change between two consecutive lateral levels takes place. For instance, the first offset $o_1^l$ in the figure determines the merging area into the main highway. In

addition, the slope value $s_1^l$ at the offset point calibrates how steeply the boundary moves from $y_1^l$ to $y_2^l$.

In general, for each boundary of an itinerary, the user needs to provide a set of $P+1$ lateral level values $\mathbf{y} \in \mathbb{R}^{P+1}$, along with a set of $P$ corresponding offset values $\mathbf{o} \in \mathbb{R}^P$ and slope values $\mathbf{s} \in \mathbb{R}^P$. As mentioned, the hyperbolic tangent function enables gradual change of the boundary from each $y_p$ to $y_{p+1}$, with steepness at offset $o_p$ being regulated by the slope value $s_p$. Using these sets of parameters, each vehicle can obtain the boundary's (left or right) lateral placement $y_b(x)$ at any longitudinal position $x$ and incorporate this into its movement strategy (see Section 4). The calculation of $y_b(x)$ follows the equation below:

$$y_b(x) = \sum_{p=1}^{P} \left[ \frac{y_{p+1} - y_p}{2} \tanh\left(s_p (x - o_p)\right) \right] + \frac{y_1 + y_{P+1}}{2} \tag{15}$$

where the summation involves all provided elements $\forall p \in [1, P]$, while the constant term shifts the resulting sum to yield the proper lateral position of the boundary.

Equation (15) can be better understood through the following two examples. Considering a boundary with $P$ offset points, we look for the boundary's position $y_b(x)$ for $o_m < x < o_{m+1}$, where $m \in [1, P]$ is an offset index. When $x$ is not too close to any offset, we have $\tanh(s_p(x - o_p)) \approx 1, \quad \forall p \in [1, m]$, and $\tanh(s_p(x - o_p)) \approx -1, \quad \forall p \in [m+1, P]$. As such, the equation above results in:

$$y_b(x) \approx \left(\frac{y_2 - y_1}{2} + \ldots + \frac{y_{m+1} - y_m}{2} - \frac{y_{m+2} - y_{m+1}}{2} - \ldots - \frac{y_{P+1} - y_P}{2}\right) + \frac{y_1 + y_{P+1}}{2} \tag{16}$$

which yields $y_b(x) \approx y_{m+1}$, meaning that, when sufficiently far from offset points, the boundary corresponds to level $y_{m+1}$, see, e.g., the straight road level $y_2^l$ in Fig. 2. Another indicative case refers to the value of $y_b(x)$ when a vehicle crosses an offset, i.e., at $x = o_m$. Assuming that the nearby offsets are not too close, then $\tanh(s_p(x - o_m)) \approx 0$ while the tangent functions for all other $p \neq m$ are close to either $+1$ or $-1$, as in the previous example. Following this, we get $y_b(x_m) \approx (y_m + y_{m+1})/2$, i.e., the boundary's lateral position at offsets is approximately in the middle of the two adjacent levels, see Fig 2. Note that offset points are inflection points of the formed curve $y_b(x)$ in (15).

If needed, it is possible, within TrafficFluid-Sim, to design asymmetric lateral level changes via selection of yet another set of parameters $\mathbf{n} \in \mathbb{R}^P$. Then, at offset $o_p$, the boundary is placed

approximately at $n_p \cdot (y_p + y_{p+1})$, where $n_p \in (0,1)$. Asymmetric changes for the lateral levels may be useful when designing boundaries within limited space. Note that for such asymmetric lateral changes $(n_p \neq 0.5)$, equation (15) delivering $y_b(x)$ is accordingly generalized.

### 3.2 Microscopic IBC Loop

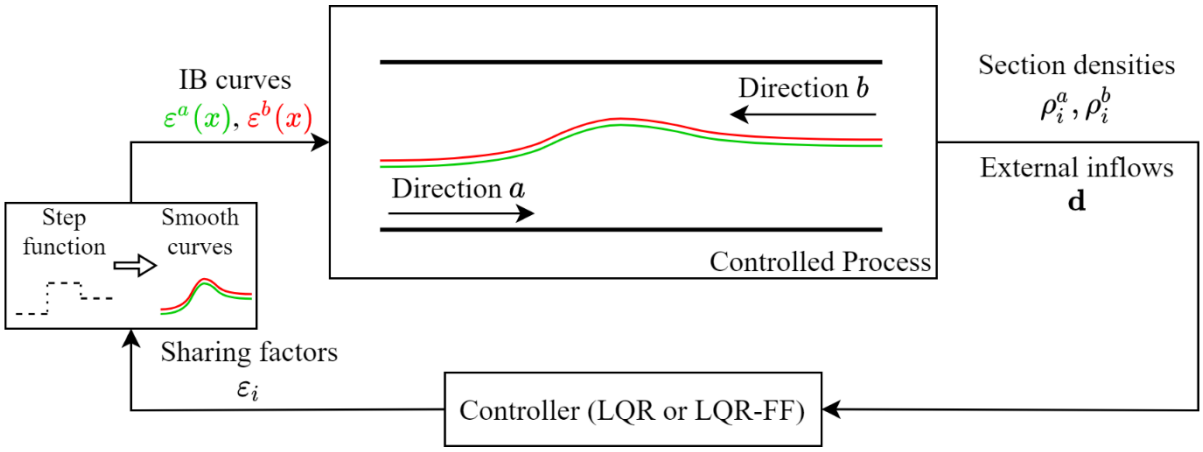


Fig. 3: Overview of the IBC closed-loop system

The control loop that involves the controlled traffic process and the controller (LQR or LQR-FF) for IBC is provided in Fig. 3, where the loop is updated with time interval $T_c$. The controlled process in this study is the microscopic simulation environment which reflects a potential real-world system. In the microscopic context, the controller output needs to be transformed to a smooth Internal Boundary (IB) curve for the traffic process, while the latter provides real-time measurements of density and external inflows (only for LQR-FF) to the controller.

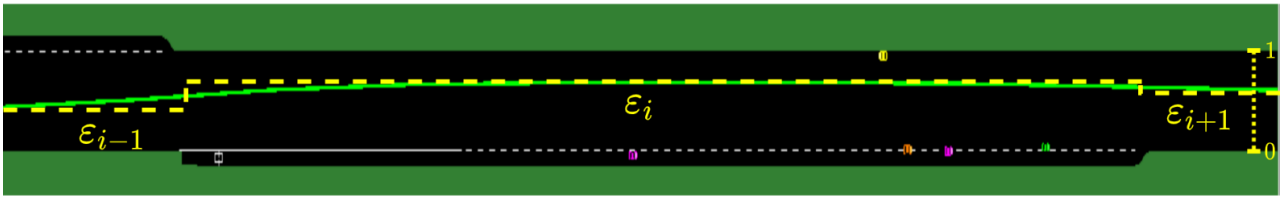


Fig. 4: Transformation of IBC controller output to the smooth internal boundary.

As discussed in Section 2, the controller (eq. (9) or (14)) outputs sharing factor values $\varepsilon_i$ per highway section $i$, i.e., a step-function of longitudinal space $x$. For both the real system and our microscopic simulation, this step-function must be transformed to a continuous and smooth IB curve of space $x$, as illustrated in Fig. 4 for a section $i$, where the provided sharing factors $\varepsilon_{i-1}$, $\varepsilon_i$, $\varepsilon_{i+1}$ are seen to form a step-function (indicated with a dashed yellow line) since each

of them is associated with a corresponding section. To transform this step-function to a smooth one (green line), we use the same sigmoid function of Section 3.1, whereby the offsets points are naturally set at the borders of the highway sections used for the controller design (see Section 2); while the lateral levels $y_i$ are updated according to the values of the sharing factors $\varepsilon_i$, based on the road width.

Since the controller is applied in a microscopic environment, some safety-related aspects emerge and need to be considered while converting sharing factors to IB curves. First, a small lateral distance margin ($0.5$ m) is placed between the two traffic directions, so that vehicles travelling near the IB retain a safety distance from the opposite traffic direction. As a result, two IB curves $\varepsilon^a(x), \varepsilon^b(x)$, colored in Fig. 3 green and red, respectively, are produced, corresponding to the two directions $a, b$. In addition, while the controller updates its output according to the control time interval $T_c$ (e.g. every 1 min), a time delay in applying the sharing factor is introduced, in every section $i$, for the direction that is widened, so as to leave time to the vehicles of the narrowed direction to evacuate the shifted IB zone. This was already mentioned in Section 2.1 and led to the equations (3), where the time-delay was set equal to $T_c$. In the microscopic simulation environment, it was observed that lane-free driving CAV subtly and safely evacuate internal road zones assigned to the other traffic direction, while, on the widened road side, CAV efficiently exploit additional road zones assigned to their direction. In fact, a smaller delay is sufficient for vehicles travelling on the narrowed direction to comply with the reduced lateral space, hence a time-delay of $T_c / 2$ was adopted.

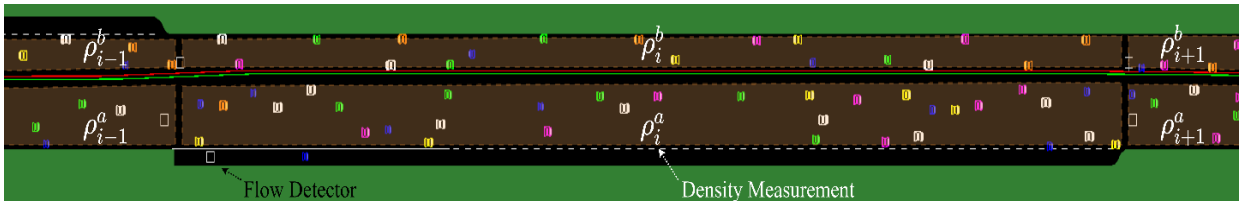


Fig. 5: Density measurements at two sections of the highway

Finally, as shown in Fig. 3 as well as in (9) and (14), the controller requires real-time information regarding density ($\text{veh}/\text{km}$) per section $i$ for each direction $a, b$. Such density measurements $\rho_i^a$, $\rho_i^b$, shown in Fig. 5, may be picked from the simulator by counting the corresponding numbers of vehicles in directions $a, b$ and dividing by the section length; and may be readily obtained in a real environment based on appropriate vehicle messages or

estimators, see e.g. (Papadopoulou, et al., 2018). The relative desities $\tilde{\rho}_i^a(k)$, $\tilde{\rho}_i^b(k)$ that are relevant to the controller may then be computed according to equation (4) using the last sharing factor values. For LQR-FF, the external inflows $\mathbf{d}(k)$ are measured using loop detectors at the network's entries, e.g. at the on-ramp in Fig. 5.

In summary, the above designn and specifications are in line with the actual IBC environment and promote a smooth driving experience. In contrast to the macroscopic testing in previous works, there is hardly any assumption dictated by the simulator; to the contrary, the simulator was enabled to reflect all necessary IBC procedures at the microscopic level.

## 4. Vehicle Movement Strategy

Developing a safe and effective approach for the movement of vehicles in a lane-free traffic environment is a complex problem (Yanumula et al., 2023, Naderi et al., 2022). In order to quickly demonstrate and verify the TrafficFluid concept, an ad-hoc vehicle movement strategy for lane-free roads was developed and demonstrated for a ring-road by Malekzadeh et al. (2022). This section outlines briefly this scheme and the necessary changes made for operation when on-/off-ramps are present.

A double-double-integrator (DDI) model is used for the vehicle motion dynamics, consisting of the following two-dimensional kinematic equations that describe the vehicle's longitudinal and lateral position and speed

$$\begin{aligned} x(t+T_v) &= x(t) + v_x(t)T_v + 0.5\, f_x(t)T_v^2 \\ v_x(t+T_v) &= v_x(t) + f_x(t)T_v \\ y(t+T_v) &= y(t) + v_y(t)T_v + 0.5\, f_y(t)T_v^2 \\ v_y(t+T_v) &= v_y(t) + f_y(t)T_v \end{aligned} \tag{17}$$

for $t = 0, T_v, 2T_v, \ldots$ Thus, at the beginning of each time-step $t$ of length $T_v$, each vehicle departs from position $(x(t), y(t))$, that is actually the center of the vehicle, with longitudinal (lateral) speed $v_x(t)$ $(v_y(t))$; and, moving with constant longitudinal (lateral) acceleration $f_x(t)$ $(f_y(t))$, it reaches its updated state (positions and speeds) at time $t+T_v$. In the above equations, the acceleration value is considered as a control input to be specified by the moving strategy. The DDI model is deemed appropriate for vehicle movement that does not involve strong turnings, as is typically the case on highways.

In the employed vehicle movement strategy, longitudinal (x-direction) and lateral (y-direction) accelerations for each CAV at time $t$ are computed via the following equations:

$$\begin{aligned} f_x(t) &= \sigma_x^{ts} f_x^{ts}(t) + f_x^{rp}(t) + \sigma^{ng}\gamma_x f_x^{ng}(t) \\ f_y(t) &= f_y^{ts}(t) + f_y^{rp}(t) + \sigma^{ng}\gamma_y f_y^{ng}(t) \end{aligned} \tag{18}$$

A brief account of the role of each "force" on the right-hand side of (18) is provided here:

- The *target-speed forces* $f_x^{ts}$ and $f_y^{ts}$ strive for the vehicle to attain its respective longitudinal and lateral target speeds. $f_x^{ts}$ is not active all the time. Whether this term is activated or not is contingent on the vehicle's relative position to other vehicles in its vicinity. Activation or deactivation of $f_x^{ts}$ is performed using the binary variable $\sigma_x^{ts} \in \{0,1\}$.
- The *repulsive forces* $f_x^{rp}$ and $f_y^{rp}$ are present to prevent any crashes from happening with vehicles ahead (downstream).
- The *nudging forces* $f_x^{ng}$ and $f_y^{ng}$ are present due to vehicles behind (upstream) and may facilitate advancement of faster vehicles behind, but have also an impact on the macroscopic characteristics of the emerging traffic flow (Karafyllis et al., 2022). The coefficients $\gamma_x, \gamma_y \in [0,1]$ regulate the influence of nudging forces versus repulsive forces, enabling attenuation of nudging forces if desired. The nudging forces $f_x^{ng}$ and $f_y^{ng}$ may under circumstances have to be de-activated, and this is performed using the binary variable $\sigma^{ng} \in \{0,1\}$.

Fig. 6 visualizes repulsive and nudging forces between two adjacent vehicles $i$ and $j$ in lane-free traffic. A repulsive force $f_j^{rp}$ is created for each couple of adjacent vehicles, with a direction along the line connecting both vehicle centers. The repulsive force indicates towards, and applies to, the vehicle $i$, whose center is farther upstream. Its magnitude depends on the distance, relative speed and lateral displacement of both vehicles and is partly inspired by lane-based car-following ACC (Adaptive Cruise Control) laws. The downstream vehicle $j$ receives a nudging force $f_i^{ng}$ with opposite direction and equal magnitude to the repulsive force $f_j^{rp}$, which, however, can be moderated by the choice of the aforementioned parameters $\gamma_x, \gamma_y$.

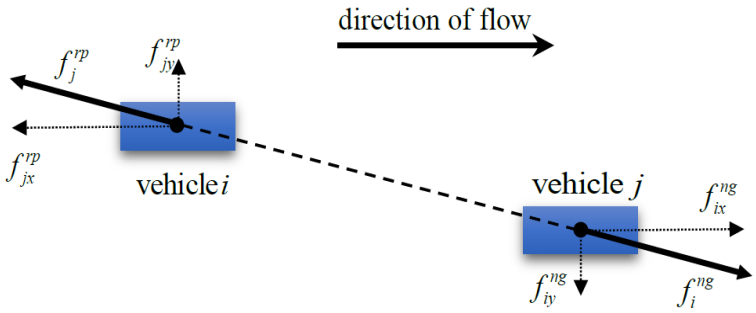


Fig. 6: Visualization of repulsive and nudging forces between two vehicles.

The total repulsive force $f^{rp}$, acting on a reference vehicle, equals the sum of the four strongest-in-magnitude individual repulsive forces due to vehicles within a downstream longitudinal distance. Similarly, the nudging force $f^{ng}$, acting on a reference vehicle, equals the sum of two strongest-in-magnitude individual nudging forces due to vehicles within an upstream longitudinal distance. After $f_x$ and $f_y$ have been produced from the respective sums of target-speed, repulsive and nudging forces via (18), a constraining mechanism is applied before they are used as accelerations. In particular, in order to keep a vehicle within the boundaries of the highway, lateral acceleration bounds are computed through a regulation problem, whereby a (left or right) road boundary is considered as a reference lateral position, and a lateral acceleration of the vehicle is obtained via a boundary feedback controller, such that the vehicle moves asymptotically towards the boundary, or remains on the boundary, without violating it. Consequently, such an acceleration can be used as a lateral acceleration bound to ensure that the vehicle will never cross the corresponding road boundary. Other bounds are applied as well, e.g. to avoid the backward moving of vehicles, to avoid speeds that exceed excessively the desired (target) speeds, etc.

A comprehensive explanation of the relations leading to the aforementioned forces can be found in (Malekzadeh et al., 2022). The simulation results presented in that work considered a ring-road without any on-ramps or off-ramps. However, to study the effect of congestion creation due to merging and the related spillback caused, the present work considers the presence of on-ramps and off-ramps, and therefore, the moving strategy was appropriately extended compared to (Malekzadeh et al., 2022). Specifically, while vehicles travelling on the mainstream have

zero lateral target (desired) speed, vehicles travelling towards a deceleration lane that leads to an off-ramp; or vehicles travelling on an on-ramp and trying to merge to the mainstream through an acceleration lane are assigned a negative or a positive desired lateral speed, respectively, to enable corresponding smooth exiting or entering maneuvers. Also, exiting or entering vehicles have extended road boundaries near the acceleration and deceleration lanes (according to Section 3.1, see also Fig. 2). It is important to note that all smooth boundaries intended for vehicle entry, exit, and road width adjustments are parametrized and can be readily adjusted if needed.

## 5. Simulation Investigations

### 5.1 Simulation Set-Up, Control Parameters and Demand Scenario

The bi-directional highway stretch displayed in Fig. 7 is used to test and analyse the IBC control scheme proposed. This highway is 3 km long and was divided into six sections, each being 0.5 km long, for LQR design and IBC application according to Section 2. When deciding on the section lengths, two points need to be taken into account. Firstly, sections are utilized for modelling within the discrete CTM, in which the length of 0.5 km is deemed to be suitable for the purpose, see (Kontorinaki et al., 2017). Secondly, the sections are utilized for IBC, to specify the scope of every sharing factor. If the sections are too long, the flexibility of IBC might be affected; while shorter sections would necessitate accordingly more frequent vehicular maneuvers to adapt to the changing IB. In light of these factors, the decision was made to use a section length of 0.5 km, but other section lengths in this order may also be used, e.g. to adapt to the roadway geometry (for example the position of on-ramps and off-ramps in each direction or changes in total road width) and the typical traffic situations. The investigated highway comprises one on-ramp and one off-ramp per direction (Fig. 5), yielding an inhomogeneous traffic situation in both space and time.

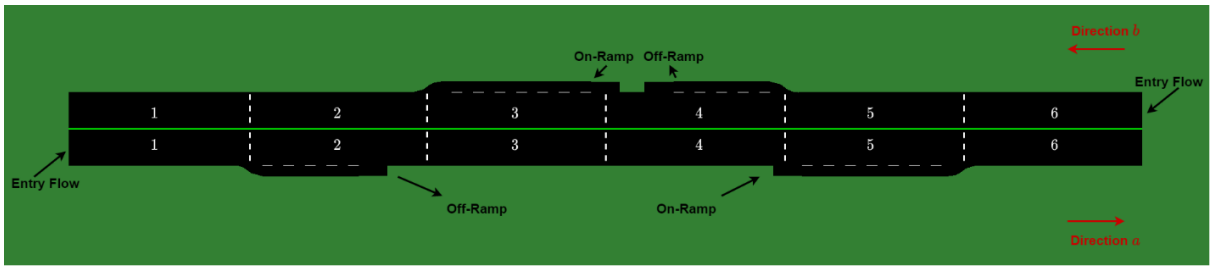


Fig.7: The considered stretch of highway

With regard to the microscopic simulation, the vehicle movement strategy is employed with a time step of 0.2 s. The dimensions of the vehicles are determined by choosing randomly (with uniform distribution) one out of the six "dimension classes" reported in Table 1. Also, the desired longitudinal speed assigned to a vehicle is chosen randomly (with uniform distribution) within the range [25, 35] m/s = [90, 126] km/h.

Table 1. The different dimension classes of vehicles applied in the simulation

| | Class 1 | Class 2 | Class 3 | Class 4 | Class 5 | Class 6 |
|---|---|---|---|---|---|---|
| Length (m) | 3.20 | 3.90 | 4.25 | 4.55 | 4.60 | 5.15 |
| Width (m) | 1.60 | 1.70 | 1.80 | 1.82 | 1.77 | 1.84 |

As outlined in Section 2, the relative density is a key factor in IBC design and scope. According to (4), the relative density depends on the total critical density of the road. Based on the CTM calibration reported in (Papamichail, et al. 2023) with a triangular fundamental diagram, the model parameters used for control design have the following values: $q_{cap} = 28{,}000\,\text{veh/h}$, $\rho_{cr} = 360\ \text{veh/km}$, $v_f = 95\,\text{km/h}$.

Initializing the LQR (9) or (14) requires the control input (sharing factor) values to be set to the nominal values, i.e. 0.5 for all sections. The highest and lowest admissible values for the sharing factors, used to prevent complete blocking in either direction, are identical throughout $i = 1, 2, \ldots, 6$ and given the values $\varepsilon_{lb} = 0.1$ and $\varepsilon_{ub} = 0.9$. Sharing factors delivered by the IB controller are truncated if they exceed these bounds. The weighing matrices of the objective

function are chosen $\mathbf{Q} = \mathrm{diag}(\mathbf{S}_1, \mathbf{S}_2, \ldots, \mathbf{S}_n)$ where $\mathbf{S} = [\mathbf{I}_2, \mathbf{0}_{2\times 1}; \mathbf{0}_{1\times 3}], \mathbf{R} = \mathbf{I}_{n\times n}$. These weights were specified empirically, but sensitivity of the control performance with respect to the weight values is low, see also (Malekzadeh, et al. 2021b). The used control sample time is $T_c = 60\,\mathrm{s}$.

The employed mainstream and on-ramp demand trajectories for each direction are presented in Fig. 8, for a time horizon of 90 min. While the on-ramp demands are relatively low, the mainstream demand feature strong peaks, which are displaced in time for the two directions, so as to highlight the working and benefits of IBC. Notice the high-frequency fluctuation, which is natural in highway demands and flows.

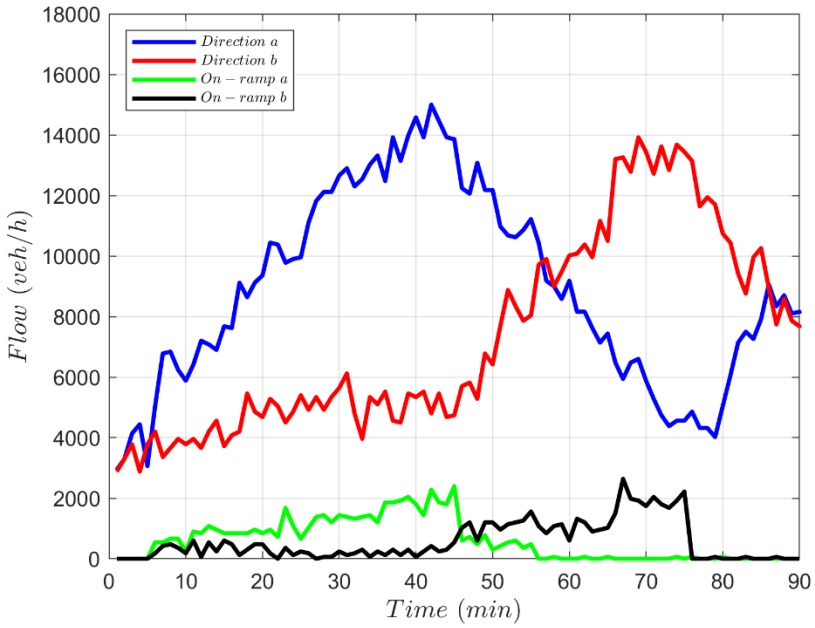


Fig. 8: Upstream and on-ramp demands per direction

When IBC is activated, the controller uses the relative densities to compute in real-time the IB curves. As a result of the high-frequency demand fluctuation, which is transferred also to the density measurements and relative density values, the control input resulting from the feedback loop may also exhibit some fluctuation, which would not be conducive to IBC application. Real-time IBC requires that the control signal features (if at all) negligible noise. This is because we don't want to see the internal boundary moving forth and back, for obvious reasons, but we want it to reflect the short-term trend in the real-time measurements. There are various possible ways to achieve this, and exponential smoothing is the simplest one, hence the collected measurement fluctuations are mitigated via an exponential filter

$$\mathbf{x}^{sm}(k_c) = \alpha_1 \mathbf{x}(k_c) + (1-\alpha_1)\mathbf{x}^{sm}(k_c - 1) \tag{19}$$

before using them for feedback control. For the same reason, exponential filtering is also applied to the external demands used in the feedforward term of LQR-FF

$$\mathbf{d}^{sm}(k_c) = \alpha_2 \mathbf{d}(k_c) + (1-\alpha_2)\mathbf{d}^{sm}(k_c - 1)\,. \tag{20}$$

where $0 \le \alpha_1, \alpha_2 \le 1$ .The smoothing yields a more moderate control reaction and even some delay in following the trend of the measurements. Therefore, while choosing the smoothing parameter, we face a trade-off of control noise versus control adaptation to trends. Such trade-off is typically addressed via trial-and-error (sensitivity investigation), which we carried out to specify a smoothing parameter that satisfies both aspects at sufficient level. The value $\alpha_1 = \alpha_2 = 0.5$ was found appropriate and is used in the reported investigations. Note that there are alternative or additional possibilities to suppress noise which were not employed since the simple exponential smoothing was found sufficient.

### 5.2 Investigation Results

When no IBC is applied, hence the total mainstream width of the road is shared equally among the two traffic directions, congestion is created in both of them, displaced in time according to the demand peaks of Fig. 8. Congestion in each direction is created at the respective on-ramp sections, when the increasing mainstream demands of either direction plus the respective on-ramp flows exceed the respective (equal) road capacities, i.e. yield densities higher than the respective (equal) critical densities. A graphical representation of the spatio-temporal changes of the relative density in the two directions can be seen in Fig. 9. Recall that relative density values lower than 1 are indicative of non-congested traffic; whereas values exceeding 1 signify congested traffic. If the relative density is around 1, and the downstream section is free-flowing, then we have capacity flow in the relevant section.

Figure 9 illustrates a high level of congestion in section 5 for direction $a$, caused by the merging on-ramp inflow with the increased mainstream demand, at around $t = 40\,\text{min}$. The tail of the created congestion travels upstream, until it ultimately reaches section 1. Eventually, the congestion dissolves at around $t = 55\,\text{min}$, owing to the reduction of the mainstream demand for this direction (Fig. 8). In direction $b$, the combination of the on-ramp flow and the increasing mainstream demand leads also to a congestion in section 3 at around $t = 70\,\text{min}$. The congestion propagates upstream to section 5 and dissolves at around $t = 80\,\text{min}$.

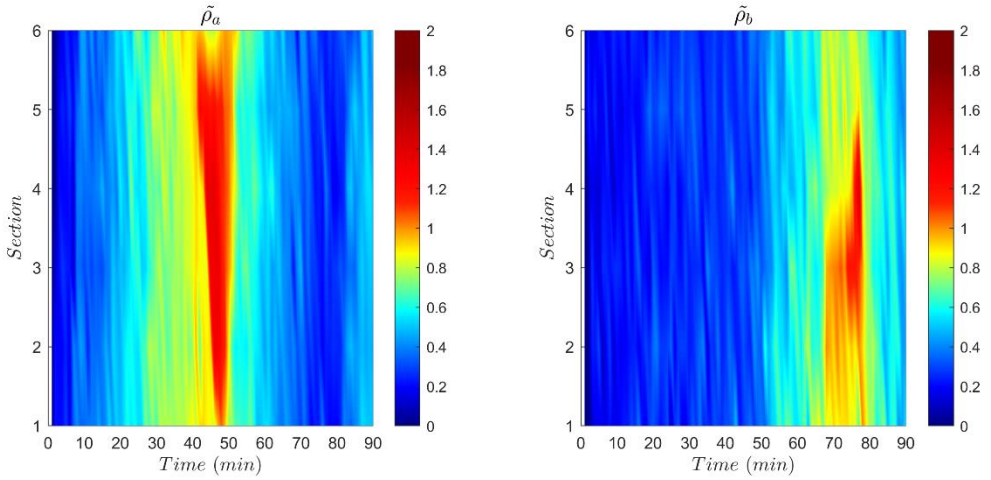


Fig. 9: Relative density for the two directions in the no-control case

Turning to the control cases, our investigation has two main aims: First, to test and demonstrate the previously developed LQR (9) for IBC in a realistic microscopic environment; second, to investigate on possible benefits provided by its extension, introduced in this paper, with a feedforward term (LQR-FF) in (14).

Figures 10 and 11 depict the spatio-temporal evolution of the relative densities with LQR and LQR-FF control, respectively. Further insights are provided from Figs. 12 and 13, which refer to the merging sections 3 and 5, respectively, where congestions appear in the no-control case. Each figure comprises four diagrams, namely for the respective flows, relative densities, mean speeds and sharing factors (control inputs), the latter along with their upper and lower bounds (black lines). Each diagram (except for the sharing factors) displays the mentioned information for both directions $a$ and $b$, and for both LQR and LQR-FF. As a first observation, the sharing factor trajectories exhibit only minor time-fluctuations, compared to the demand (Fig. 8) and relative density trajectories that feed the controllers, thanks to the smoothing (19), (20).

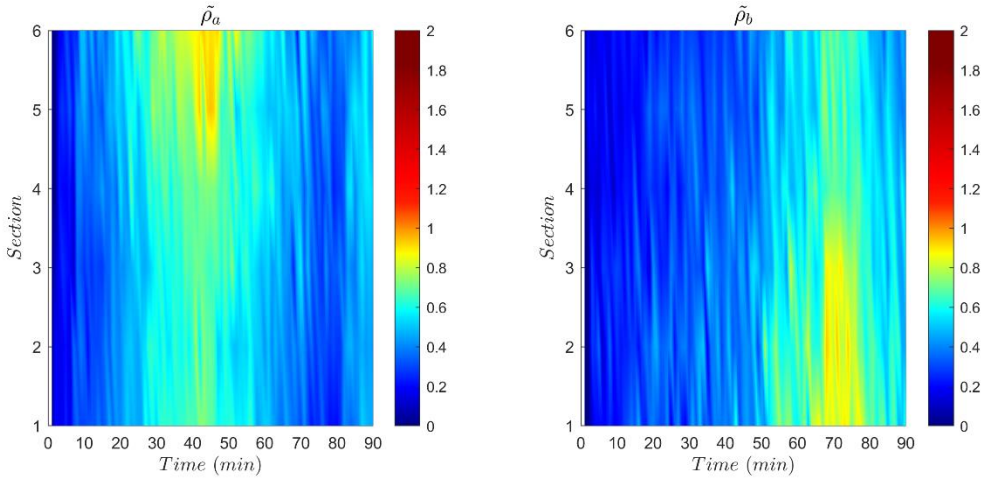


Fig. 10: Relative density for the two directions in the LQR control case

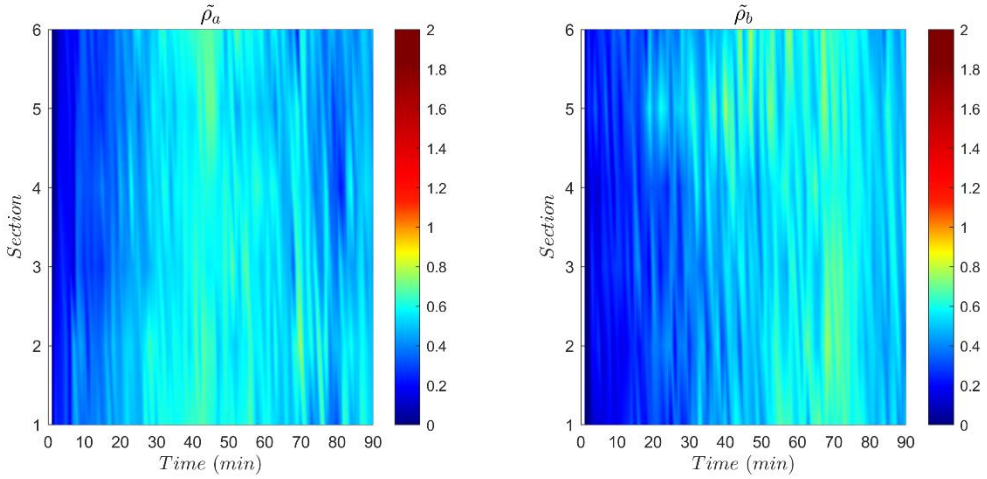


Fig. 11: Relative density for the two directions in the LQR-FF control case

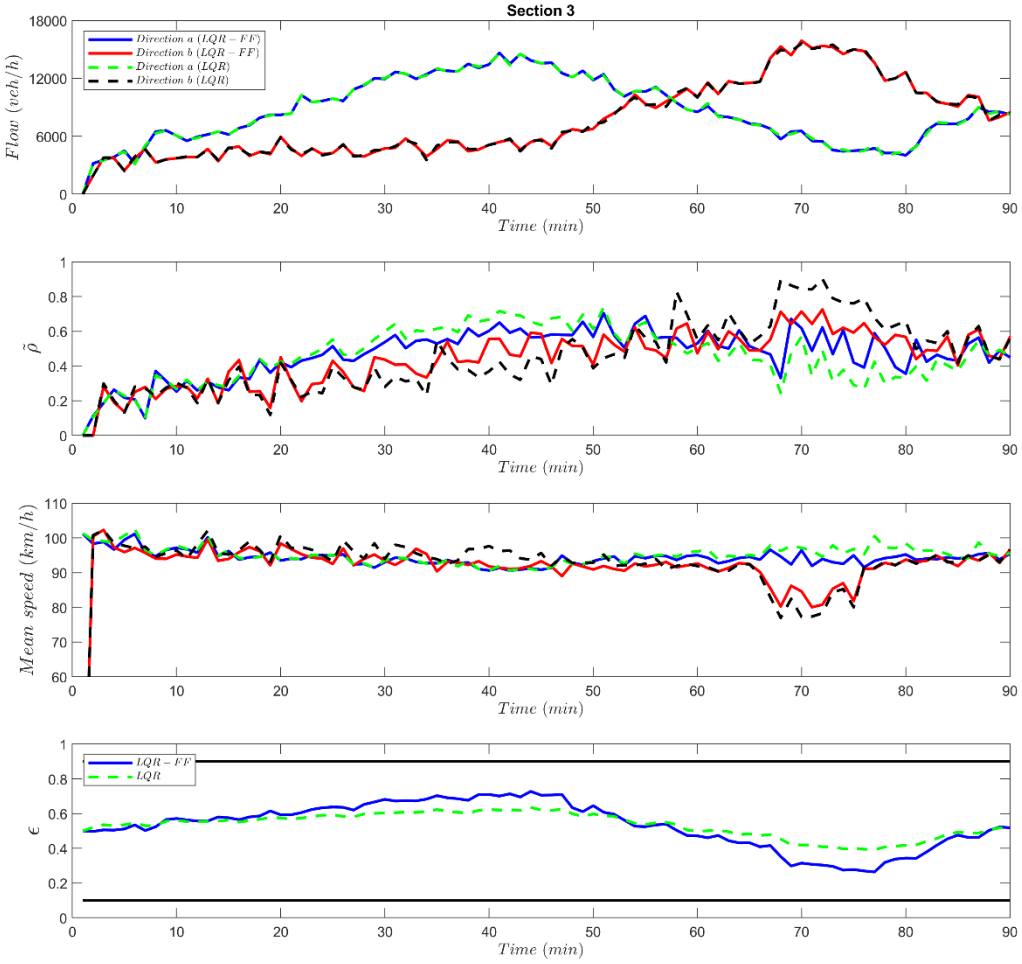


Fig. 12: Flow, relative density, mean speed and control trajectories in the control case (section 3)

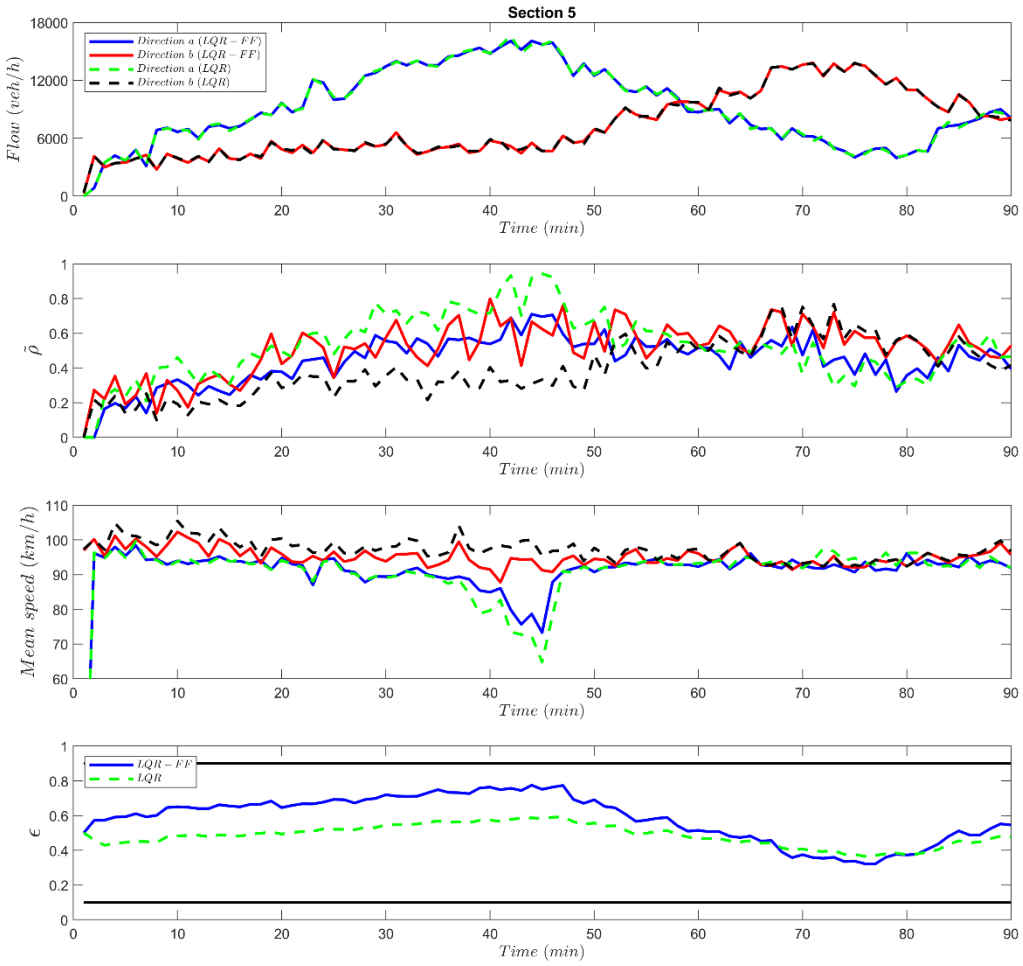


Fig. 13: Flow, relative density, mean speed and control trajectories in the control case (section 5)

All relative densities in all sections are lower than 1 for both controllers; hence traffic conditions are always and everywhere under-critical, i.e. congestion is utterly avoided, as also evidenced by the mean speed trajectories in Figs. 12 and 13. Thus, both LQR and LQR-FF appear equally successful in this respect for the considered scenario. It is worth noting that the avoidance of a no-control congestion in one direction is achieved via appropriate IB shifting towards the other direction, which yields a small RD increase in the latter, compared to the no-control case, as evidenced in Figs. 9 – 11.

Taking a closer look at the sharing factor diagrams in Figs. 12 and 13, LQR-FF is more reactive than LQR, i.e. the occurring $\varepsilon$-differences from the nominal value (0.5) are stronger. As a result, the two relative densities (RDs) in the two directions of every section are closer to each

other (see Figs. 12, 13), i.e. LQR-FF is better in balancing the RDs of the two directions. This may be further assessed with Table 2. The first three columns of Table 2 indicate that the space-time averages of RD are highest for no control, followed by LQR and LQR-FF, but the differences are limited due to two reasons: First, the created congestions in the no-control case are short-lived and contribute only moderately to the averages; second, as mentioned earlier, congestion avoidance in a traffic direction via IB shifting increases RD in the opposite direction. In contrast, clear differences are observed in the fourth column, which displays the space-time average of the absolute value of the RD difference in the two directions, i.e. of $\left|\tilde{\rho}_i^a(k) - \tilde{\rho}_i^b(k)\right|$. This column highlights, in quantitative terms, the superiority of LQR-FF in balancing the RDs in both directions, something that is the direct goal of IBC according to the objective criterion (7).

Another useful assessment criterion for control performance is the RD margin-to-congestion $m(k)$, which is defined, for each time $k$, as the smallest distance to 1 among all section RDs of both directions. Clearly, the bigger the margin, the higher the "distance" from a congested state; and $m(k) < 0$ indicates that a congestion has already occurred in at least one section and direction. Figure 14 displays $m(k)$ for the three examined cases. It is seen that for the no-control case, $m(k) < 0$ over the two periods of congestion in directions $a$ and $b$, respectively. It is also seen that $m(k)$ is mostly higher for LQR-FF than for LQR, hence, in case of stronger demand, LQR-FF has larger margin to the critical density and congestion creation. The smallest occurring value of m(k) is also depicted in the last column of Table 2, confirming the improved behaviour of LQR-FF in this respect.

Table 2. Averages of the relative density for no-control, LQR and LQR-FF cases.

| | Space-time average RD (direction $a$) | Space-time average RD (direction $b$) | Space-time average RD (directions $a$ and $b$) | Space-time average $\left\|\tilde{\rho}_i^a(k) - \tilde{\rho}_i^b(k)\right\|$ | Time average RD-margin | Minimum RD-margin |
|---|---|---|---|---|---|---|
| No-control | 0.52 | 0.43 | 0.47 | 0.33 | 0.23 | -0.45 |
| LQR | 0.48 | 0.43 | 0.45 | 0.21 | 0.31 | 0.06 |
| LQR-FF | 0.47 | 0.45 | 0.46 | 0.11 | 0.4 | 0.2 |

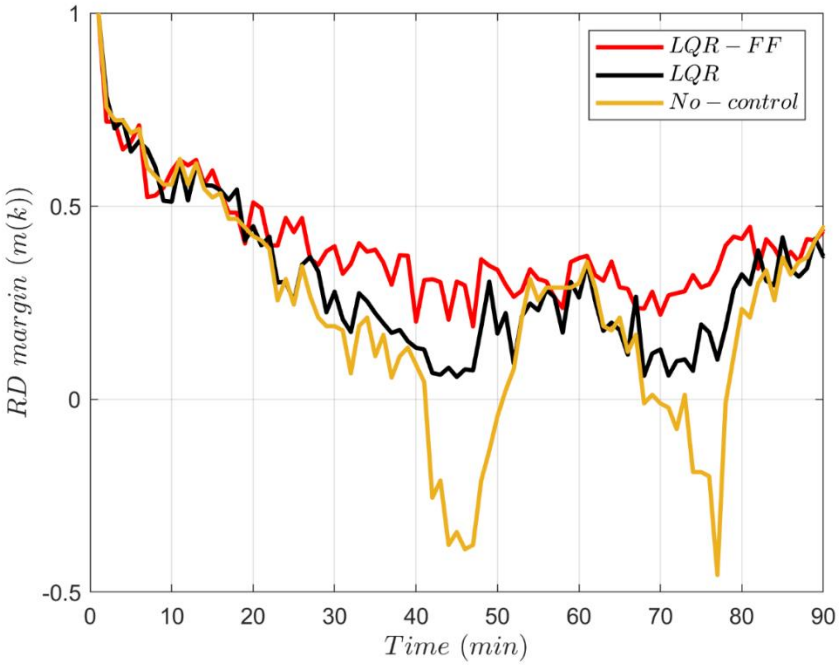


Fig. 14: The smallest (among all sections of both directions) margin of RD from 1 over time

In the macroscopic IBC testing in (Malekzadeh et al. 2021a; 2021b) by use of CTM, the mean speed is constant (free speed) for any under-critical RD due to the triangular fundamental diagram. In contrast, in the present microscopic evaluation, every increase in RD, even in the under-critical range, leads to a corresponding small decrease of the mean speed, as evidenced by Figs. 12 and 13, and also confirmed with Fig. 15 that depicts the space-average value of mean speeds for each direction and each control case over time. Clearly, in the no-control case, there is a substantial speed reduction at the period of congestion in both directions. But also for the two control cases, a small speed reduction is observed at times of increased, though under-critical, RDs. Hence, increasing the capacity for one direction (to avoid congestion) comes at a small cost for the other direction due to slightly decreased speeds. For example, consider in Fig. 15 the speeds in direction $b$ in the time window $40-50\,\text{min}$, i.e. at the period of no-control congestion in direction $a$. During this period, LQR and LQR-FF restrict direction $b$ in order to handle the increased demand on direction $a$. The impact on direction $b$ is a small speed decrease, compared to the no-control case, which is more pronounced for LQR-FF due to stronger $\varepsilon$-deviations. The same holds true also when the controllers restrict direction $a$ within the time-interval $70-80\,\text{min}$ to avoid congestion in direction $b$.

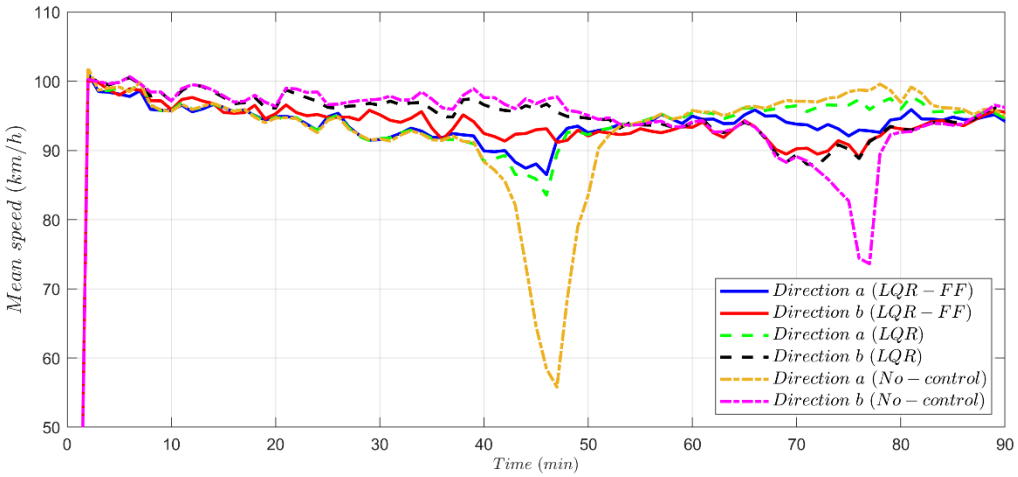


Fig. 15: Space-average of mean speeds for each direction over time for no-control, LQR and LQR-FF.

We also evaluate IBC with a well-known measure of efficiency, namely the Time Delay (TD) metric, which is depicted in Fig. 16 for 15-min time-intervals, for each direction as well as in total. TD is computed for every vehicle when it crosses the exit point and is the time difference between the actual time the vehicle spent in the network and the ideal time it would have accomplished if it was travelling at its desired speed. In the related diagrams, we provide the value of TD (in seconds) for all vehicles that have exited the network during the associated time-interval. For each time interval, you can see three boxes including LQR-FF, LQR and No-control cases. Each box is limited to two lines that connect to the box with a dashed line indicating the minimum and maximum values within each interval for each scenario. The line within the box denotes the average value of the data associated with the time interval. In addition, the bottom and top borders of the box indicate the 25th and 75th percentiles, respectively.

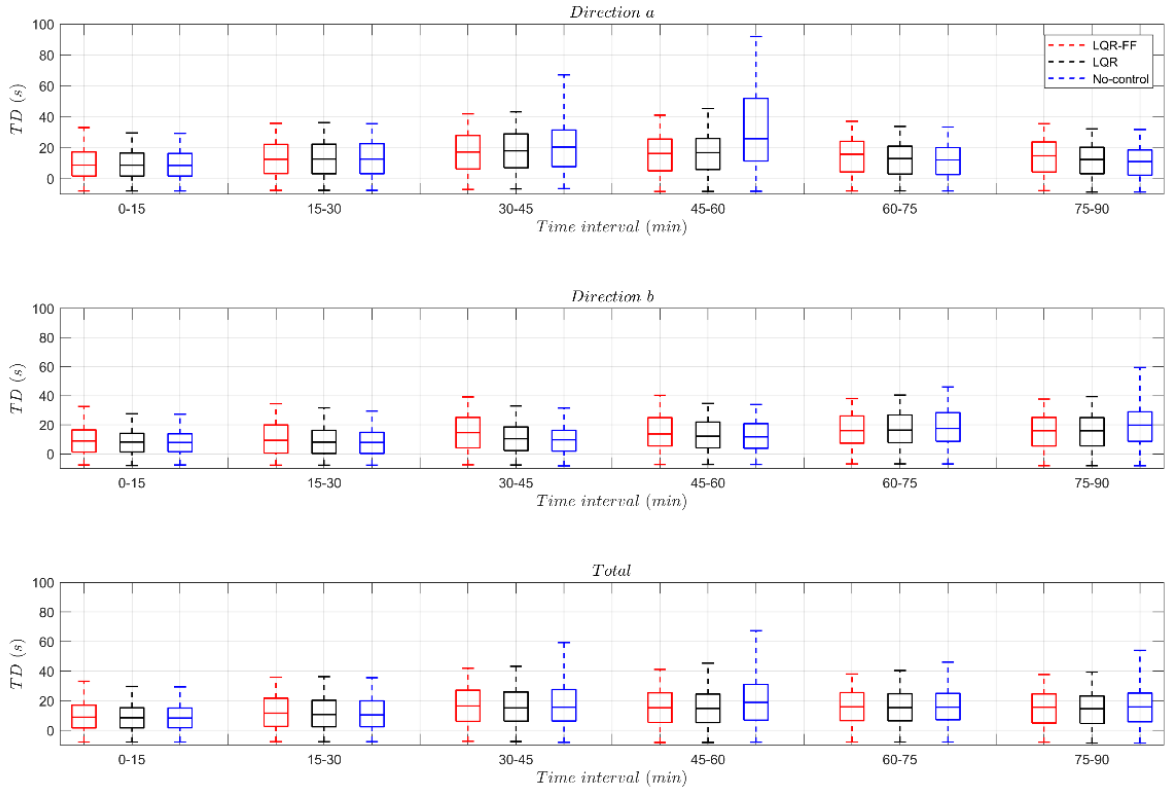


Fig. 16: Box-whisker plots of Time Delay (TD) for 15-min periods

We again compare LQR with LQR-FF and the no-control case, and the results are consistent with the comparisons on mean speed presented earlier. LQR and LQR-FF exhibit very similar performance, while the no-control results are comparable only when RDs in either direction have under-critical values. Thus, during the third and forth time-interval for direction $a$ and the fifth and sixth time-interval for direction $b$, when respective congestions occur, the no-control TD is clearly higher. In no-congestion periods, TD values may vary among the three cases in one or the other direction, depending on the respective values of the sharing factors. However, a closer look at the total TD diagram during such periods indicates a very slight increase of TD for LQR, compared to no control, and slightly more for LQR-FF. The main reason is that LQR-FF uses stronger control to better equalises the RDs of two opposite directions. The time delay associated with each change of IB has likely also an impact on this, as parts of the roadway are temporarily neutralised and remain unexplored when IBC is applied. In a nutshell, the strongly improved performance of the controllers versus no control, but also the better behaviour of LQR-FF versus LQR in balancing RDs in the two directions, come at a very low price of slightly decreased mean speeds and increased delays when traffic conditions are clearly under-critical. For this, but also for operational reasons, it is reasonable that IBC is

only switched on when a threshold of RD in either direction is exceeded, something that is practiced in many other traffic management measures as well.

Finally, Fig. 17 displays the space-time diagram of the control input, illustrating that the behaviour is consistently smooth over both space and time. Thus, vehicles driving in either direction encounter only small changes of IB on their way that may be easily accommodated (by vehicles close or on the IB) with smooth maneuvers.

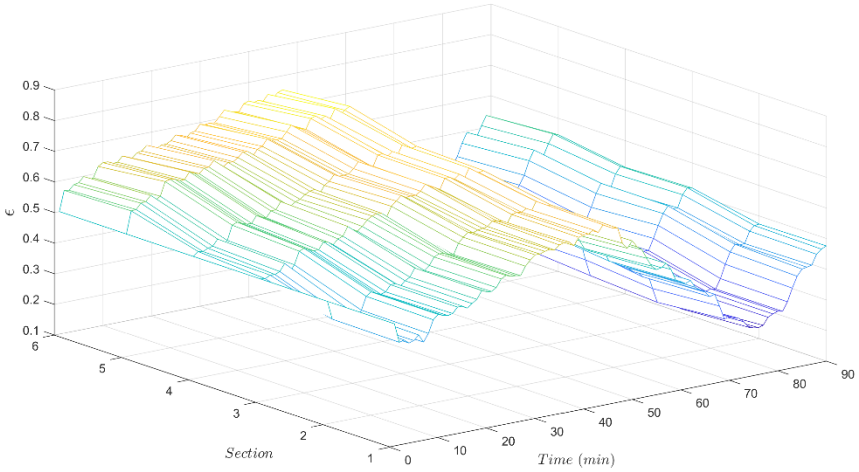


Fig. 17: Space-time diagram of the control input (LQR-FF)

Figure 5 is actually a snapshot of the microscopic simulation. Microscopic simulation videos for all three cases (no control, LQR, LQR-FF) may be viewed in this link. Watching the videos is helpful in appreciating that CAV drive safely and conveniently while encountering a smoothly changing internal boundary. Space increments (500 m) and time step (1 min) of change appear adequate.

## 6. Conclusion

This study has explored the potential use of internal boundary control for lane-free traffic on highways or arterials through microscopic simulation. The IBC scheme has been implemented by use of a previously designed LQR. In addition, a novel, extended controller, LQR-FF, incorporating a feedforward term into the LQR, was introduced, tested and compared. LQR

uses real-time measurements of the relative densities, while the feedforward term uses real-time inflow measurements at the mainstream entrance of the highway and at on-ramps. The simulation results confirm and extend previous insights and demonstrate the efficiency and feasibility of IBC in a very realistic microscopic environment. Both controllers were found to act adequately to mitigate or avoid congestion creation in cases of unbalanced demands. LQR-FF was found to offer benefits versus LQR in better balancing the relative densities in both traffic directions, thus enlarging the margin to congestion creation in case of stronger demands. Future work includes testing of the same and other control schemes, e.g. those developed by Malekzadeh et al. (2023), on longer highways and with stronger demand and traffic inhomogeneities.

**Acknowledgements**

The research leading to these results has received funding from the European Research Council under the European Union's Horizon 2020 Research and Innovation programme/ ERC Grant Agreement n. [833915], project TrafficFluid.

**References**

Courant, R., Friedrichs, K., Lewy, H., 1928. άber die partiellen differenzengleichungen der mathematischen physik. Math. Ann. 100 (1), 32–74.

Daganzo, C.F., 1994. The cell transmission model: A dynamic representation of highway traffic consistent with the hydrodynamic theory. *Transportation Research Part B: Methodological*, *28*(4), pp. 269-287.

Diakaki, C., Papageorgiou, M., Papamichail, I. and Nikolos, I., 2015. Overview and analysis of vehicle automation and communication systems from a motorway traffic management perspective. *Transportation Research Part A: Policy and Practice*, *75*, pp. 147-165.

Karafyllis, I., Theodosis, D. and Papageorgiou, M., 2022. Analysis and control of a non-local PDE traffic flow model. *International Journal of Control*, *95*(3), pp. 660-678.

Kontorinaki, M., Spiliopoulou, A., Roncoli, C. and Papageorgiou, M., 2017. First-order traffic flow models incorporating capacity drop: Overview and real-data validation. *Transportation Research Part B: Methodological*, *106*, pp. 52-75.

Kurzhanskiy, A.A. and Varaiya, P., 2010. Active traffic management on road networks: a macroscopic approach. *Philosophical Transactions of the Royal Society A: Mathematical, Physical and Engineering Sciences*, *368*(1928), pp. 4607-4626.

Lopez, P.A., Behrisch, M., Bieker-Walz, L., Erdmann, J., Flötteröd, Y.P., Hilbrich, R., Lücken, L., Rummel, J., Wagner, P. and Wießner, E., 2018. Microscopic traffic simulation using sumo. In *2018 21st International Conference on Intelligent Transportation Systems (ITSC)* (pp. 2575-2582). IEEE.

Malekzadeh, M., Yanumula, V.K., Papamichail, I. and Papageorgiou, M., 2023. Overlapping internal boundary control of lane-free automated vehicle traffic. *Control Engineering Practice*, *133*, Article105435.

Malekzadeh, M., Manolis, D., Papamichail, I. and Papageorgiou, M., 2022. Empirical investigation of properties of lane-free automated vehicle traffic. In *2022 IEEE 25th International Conference on Intelligent Transportation Systems (ITSC)* (pp. 2393-2400). IEEE.

Malekzadeh, M., Papamichail, I. and Papageorgiou, M., 2021b. Linear–quadratic regulators for internal boundary control of lane-free automated vehicle traffic. *Control Engineering Practice*, *115*, Article 104912.

Malekzadeh, M., Papamichail, I., Papageorgiou, M. and Bogenberger, K., 2021a. Optimal internal boundary control of lane-free automated vehicle traffic. *Transportation Research Part C: Emerging Technologies*, *126*, Article 103060.

Marinaki, M. and Papageorgiou, M., 2005. Optimal real-time control of sewer networks. London: Springer.

Naderi, M., Papageorgiou, M., Karafyllis, I. and Papamichail, I., 2022. Automated vehicle driving on large lane-free roundabouts. In *2022 IEEE 25th International Conference on Intelligent Transportation Systems (ITSC)* (pp. 1528-1535). IEEE.

Papadopoulou, S., Roncoli, C., Bekiaris-Liberis, N., Papamichail, I. and Papageorgiou, M., 2018. Microscopic simulation-based validation of a per-lane traffic state estimation scheme for highways with connected vehicles. Transportation Research Part C: Emerging Technologies, 86, pp.441-452.

Papageorgiou, M., Diakaki, C., Dinopoulou, V., Kotsialos, A. and Wang, Y., 2003. Review of road traffic control strategies. *Proceedings of the IEEE*, *91*(12), pp. 2043-2067.

Papageorgiou, M., Mountakis, K.S., Karafyllis, I., Papamichail, I. and Wang, Y., 2021. Lane-free artificial-fluid concept for vehicular traffic. *Proceedings of the IEEE*, *109*(2), pp.114-121.

Papageorgiou, M., Leibold, M., Buss, M., 2015. Optimierung: statische, dynamische, stochastische Verfahren für die Anwendung (Optimisation: FFApplied static, dynamic, stochastic methods), 4th Edition. Springer, Berlin.

Papamichail, I., Schoenn-Anchling, N., Malekzadeh, M., Markantonakis, V., and Papageorgiou, M., 2023. Macroscopic Traffic Flow Model Calibration for Lane-free Automated Vehicle Traffic. In *2023 IEEE 26th International Conference on Intelligent Transportation Systems (ITSC)*. IEEE.

Papamichail, I., Bekiaris-Liberis, N., Delis, A.I., Manolis, D., Mountakis, K.S., Nikolos, I.K., Roncoli, C. and Papageorgiou, M., 2019. Motorway traffic flow modelling, estimation and control with vehicle automation and communication systems. *Annual Reviews in Control*, *48*, pp. 325-346.

Rostami-Shahrbabaki, M., Weikl, S., Niels, T. and Bogenberger, K., 2023. Modeling Vehicle Flocking in Lane-Free Automated Traffic. *Transportation Research Record*, p.03611981231159405.

Yanumula, V.K., Typaldos, P., Troullinos, D., Malekzadeh, M., Papamichail, I. and Papageorgiou, M., 2023. Optimal trajectory planning for connected and automated vehicles in lane-free traffic with vehicle nudging. *IEEE Transactions on Intelligent Vehicles*.

Treiber, M. and Kesting, A., 2013. Traffic flow dynamics. Traffic Flow Dynamics: Data, Models and Simulation, Springer-Verlag Berlin Heidelberg, pp.983-1000.

Troullinos, D., Chalkiadakis, G., Manolis, D., Papamichail, I. and Papageorgiou, M., 2021. Lane-free microscopic simulation for connected and automated vehicles. In *2021 IEEE International Intelligent Transportation Systems Conference (ITSC)* (pp. 3292-3299). IEEE.

Troullinos, D., Chalkiadakis, G., Manolis, D., Papamichail, I. and Papageorgiou, M., 2022, September. Extending SUMO for lane-free microscopic simulation of connected and automated vehicles. In *SUMO Conference Proceedings* (Vol. 3, pp. 95-103).